

An Improved Hybrid Path Planning Algorithm in Indoor Environment

Jiaxiang Fang

School of Computer Science & Engineering
Xi'an Technological University
Xi'an, China
E-mail: 2293950221@qq.com

Shuping Xu

School of Computer Science & Engineering
Xi'an Technological University
Xi'an, China
E-mail: 563937848@qq.com

Abstract—During the path planning of robots in the indoor unstructured complex environment, there are often problems such as unreachable target points, deflection in the planning process, and failure to avoid dynamic obstacles in time. To solve these problems, an improved hybrid indoor path planning algorithm was proposed, wherein the improved global path planning algorithm was effectually integrated with improved local path planning algorithm. Firstly, the heuristic factor of traditional A-Star algorithm was optimized, search range and nodes were reduced, and then the path generated by traditional A-Star algorithm for path planning was smoothed using the angle bisector tangent point method. Secondly, combining path and environment information, local path planning was undertaken by utilizing the improved artificial potential field algorithm, and the unreachable target points problem was addressed by adjusting the repulsive field parameters. Additionally, dynamic potential field function was constructed to make it have the ability to resolve dynamic obstacles. Finally, in the part of actual environment verification, a comparison was made in this paper to assess the performance of the traditional hybrid algorithm against the improved algorithm in terms of path planning. The consequences showed that, by the hybrid algorithm proposed in this paper, the path planning length was reduced by 10.3%, the running time was decreased by 12.5%, and 34 redundant nodes were eliminated. The consequences indicated that the hybrid algorithm can effectively address the indoor unstructured and complex path planning problems.

Keywords-Mobile Robot; Path Planning Technology; A-Star Algorithm; Artificial Potential Field Algorithm; Autonomous Obstacle Avoidance

Driven by the swift evolution of technology, indoor mobile robot path planning has become a topic of keen interest in the research community. In essence, mobile robot path planning is in the case of excluding human manipulation, the mobile robot identifies and processes the data obtained by

the sensor, and calculates an optimal path which is safe and collision-free at the same time [1]. At present, the widely used global path planning algorithms currently include A-Star algorithm [2], D-Star algorithm [3], etc. Frequently applied algorithms for local path planning are the artificial potential field method [4], dynamic sliding window method [5], fuzzy logic method [6], etc. A-Star algorithm is a well-known global path planning algorithm, which is a heuristic algorithm [7] that mainly uses heuristic information to find the optimal path [8]. The optimal path is selected by the artificial potential field algorithm in a manner that the potential function decreases within the obstacles force field.

The A-star algorithm excels in its direct search methodology, effectively delivering satisfactory planning solutions, but it is plagued by poor real-time performance and issues such as deviation caused by turning angles. The artificial potential field method stands out as a prominent local path planning technique. It boasts simplicity in calculation and analysis, easy control, and superior real-time performance. However, it is prone to issues such as local minima and unreachable targets. Moreover, both of them cannot get satisfactory results in the treatment of dynamic obstacles. To address these problems, relevant scholars have proposed various improvements and optimizations to the algorithm. For instance, literature [9] described a bidirectional time-efficient A-Star algorithm for path finding, employing a multi-neighbor grid distance calculation scheme to achieve improved efficiency and smoother paths. However, this approach tends to deviate during navigation when dealing with

large, complex maps. Literature [10] avoided generating paths through obstacle grid vertices by adding a priority-based child node generation strategy into the A-Star algorithm, but the path smoothness during navigation is not enough, which has certain security risks. Literature [11] improved the key node selection strategy of A-star algorithm, thus optimizing path planning in static environments to some extent, but still unable to resolve errors in dynamic environments. Literature [12] put forward an iterative searching strategy capable of skipping intermediate nodes, leading to a decrease in the number of accessed nodes and an enhancement in the overall speed of the algorithm. Nevertheless, the path still contains numerous turning points, prone to issues such as path drift. Literature [13] proposed an improved ant colony algorithm in global path search. The smoothness and calculation effect of path planning is more obvious than A-star algorithm, but the amount of data in the search process is too large to be suitable for equipment with poor performance. In terms of artificial potential field algorithms, literature [14] used the improved Pseudo-Dubins curve to smooth the path, which can obtain better local path calculation effect, but the calculation is cumbersome and the operation efficiency is poor. The study in literature [15] introduced a hierarchical modification technique to tackle the dynamic obstacle avoidance challenge in artificial potential fields, resulting in improved obstacle avoidance performance during movement. Nevertheless, it still faces issues of unreachable targets and local optima. Literature [16] proposed a method to introduce the motion direction of the robot as the control variable in the operation of the potential field function, which can effectively reduce the repulsion of obstacles other than the motion direction to the robot, eliminate the inaccessibility of unreachable target points, but increase the risk of robot collision. Literature [17] used a method of adding virtual sub target points to address the local minimum issue in potential field algorithms, but it has the shortcomings of comprehensive path planning error and excessive fold angle.

Through the above research, it can be found that in indoor unstructured complex environments,

the traditional A-Star algorithm tends to encounter path slippage and corner problems when dealing with global paths [18]; The traditional artificial potential field algorithm often fails to achieve optimal path planning results during local planning [19]. Therefore, an integrated path planning algorithm was presented in this paper, which combines an angle bisector tangent optimization for the A-Star algorithm with an enhanced artificial potential field method that constructs a dynamic force field. The improved fusion algorithm introduced ideas of angle bisector tangent points to perform global path planning based on the original A-Star algorithm. Moreover, for local planning, the utilization of an improved artificial potential field algorithm optimized the effect of obstacle avoidance when obstacles are detected during path traversal, achieving autonomous obstacle avoidance and overall path optimization. This results in a smoother path trajectory, a larger detection range, and a reduction in possible drift or errors in the path.

I. IMPROVEMENT OF A-STAR GLOBAL PATH PLANNING ALGORITHM

A. Grid map environment modeling

The construction of a grid map is the premise of mobile robot to perform path planning. Grid map is popular among scholars because of its simplicity and easy implementation. In the grid map, each grid contains information about obstacle occupancy, and each occupancy information can be represented by a specific letter, where 0 represents an occupied grid and 1 represents a free grid [20]. The grid size will affect the speed of path planning, so it is important to construct grid map reasonably.

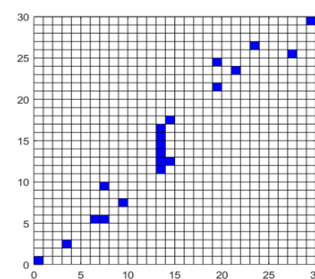


Figure 1. Raster map model

B. Traditional A-star algorithm

A-Star algorithm, as a heuristic search algorithm, incorporates a heuristic factor function into the Dijkstra algorithm to steer its search direction, thus allowing it to compute globally optimal paths in static settings [21]. The evaluation function of the A-Star algorithm is:

$$f(n) = g(n) + h(n) \quad (1)$$

The above formula is the evaluation function of A-Star algorithm. $g(n)$ is the estimated surrogate value from the starting node to the current node. It can usually be expressed by the Euclidean distance between two points.

$$h(n) = \sqrt{(x_{start} - x_{end})^2 + (y_{start} - y_{end})^2} \quad (2)$$

In the above formula, $(x_{start} - x_{end})$ represents the abscissa distance between the current node and the target node, and $(y_{start} - y_{end})$ represents the ordinate distance.

C. Improvement of A-star algorithm

The traditional A-star algorithm can plan an effective optimal path, but there are problems with too many redundant nodes and unsmooth paths. However, heuristic factor can effectively guide the search direction of the A-star algorithm. Therefore, this paper first optimized the heuristic factor function, and then smoothed the A-Star algorithm path.

1) Optimization of heuristic factors

Heuristic factor plays a key role in optimal path planning, which can guide the search direction of A-star algorithm. When $h(n) = 0$, A-star algorithm is equivalent to Dijkstra algorithm; When the estimated generation value of the heuristic factor $h(n)$ is less than the real cost value, the search range of A-star algorithm becomes larger and the number of search nodes becomes more, which can ensure the generation of the optimal path; When the estimated generation value of the heuristic factor $h(n)$ is greater than the actual cost value, the search range of A-star algorithm becomes smaller, the number of search nodes becomes less, which cannot ensure the generation of the optimal path. Seeking more realistic path planning results, the optimized heuristic factor $h(n)$ was introduced as follows:

$$h(n) = \begin{cases} \sqrt{2}|y_s - y_{end}| + |x_s - x_{end}| - |y_s - y_{end}|, & |y_s - y_{end}| \geq |x_s - x_{end}| \\ \sqrt{2}|x_s - x_{end}| + |y_s - y_{end}| - |x_s - x_{end}|, & |y_s - y_{end}| < |x_s - x_{end}| \end{cases} \quad (3)$$

2) Smooth path processing

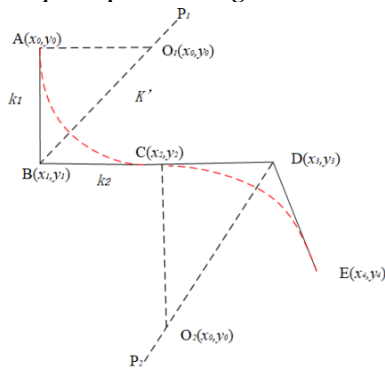


Figure 2. A-Star algorithm smoothing processing diagram

Since the traditional A-Star algorithm has an unsmooth path problem in the path planning process, the optimization method of tangent point of angle bisector was introduced to optimize the A-star algorithm, which helps generate smoother paths. The optimization model is shown in Fig. 2.

Assuming that the initial node position of the mobile robot is $A(x_0, y_0)$, the turning point is smoothed in turn, and the turning points B and D are smoothed in turn until reach the end point $A(x_i, y_i)$. The following are the steps for path optimization:

Step 1: determine if the three points are collinear, that is, if the node is a turning point. Make a vertical line crossing the angle bisector at the previous node of the turning point. In the figure above, the slope of edge AB is k_1 , the slope of edge BC is k_2 , and the slope of the angle bisector of the turning angle is denoted as k' . Where:

$$k_1 = \frac{y_2 - y_1}{x_2 - x_1}, k_2 = \frac{y_3 - y_2}{x_3 - x_2}, k_n = \frac{y_{n+1} - y_n}{x_{n+1} - x_n} \quad (4)$$

According to the slope relation formula $\frac{k' - k_1}{1 + k_1 \cdot k'} = \frac{k_2 - k'}{1 + k_2 \cdot k'}$, the expression of the slope k' of BO_1 is as follows:

$$k'^2 + \frac{2(1 - k_1 k_2)}{k_1 + k_2} \cdot k' - 1 = 0 \quad (5)$$

Then, the coordinates of the intersection point O_1 is:

$$\begin{cases} x_0 = \frac{x_1 + k_1 y_1 + k_1 (k' x_2 - y_2)}{1 + k_1 k'} \\ y_0 = k' (x - x_0) + y \end{cases} \quad (6)$$

Step 2: make a circle with the vertical length as the radius through the intersection O_1 , and judge whether there is an intersection with the tangent circle. The tangent circle equation is:

$$(x - x_0)^2 + (y - y_0)^2 = r_0^2 \quad (7)$$

The radius r_0 of the tangent circle is represented as:

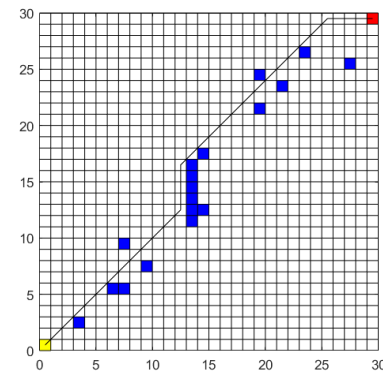
$$r_0 = \sqrt{x_0^2 + x_1^2 + y_1^2 + y_0^2 - 2x_0 x_1 - 2y_0 y_1} \quad (8)$$

Step 3: determine whether there is a next turning point. If it exists, return to step 1;

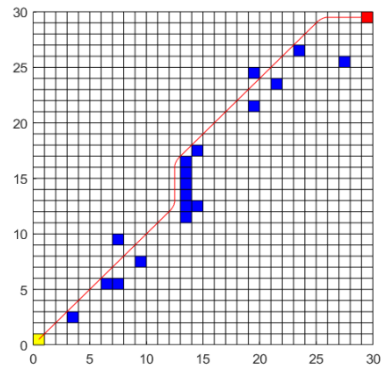
Otherwise, replace the distance between nodes with an arc.

Step 4: determine whether the optimized path contains every node from the path planned by A-star algorithm. If so, optimization process completes; Otherwise, return to step 1.

The following is a simulation experiment of the improved A-star algorithm on the grid model in Fig. 1 in MATLAB, where each grid in the abscissa and ordinate represents a distance of 1m. The verification results are as follows:



(a)Before path smoothing



(b)After path smoothing

Figure 3. A-Star algorithm path smoothing results in 30x30 environment

As evident in Fig. 3(b), compared to Fig. 3(a), the red trajectory was obviously smoothed and optimized in the trajectories of (12,12), (26,30) two meshes. By comparing various indicators in Table 1, it is evident that the improved A-Star algorithm effectively eliminated turning points, shortened the path length, improved path smoothness, reduced the time required to search for paths, and greatly reduced the number of nodes that need to be expanded during the path planning

process. This shows that the A-Star algorithm modified with the heuristic factor surpasses the

traditional A-Star in smoothness of path planning, reliability, and in judging actual trajectories.

TABLE I. COMPARISON OF THE EFFECTS OF A-STAR ALGORITHM IMPROVEMENT

Algorithm	Path length/m	Time for path finding/s	Number of expansion nodes	Is there a turning point
A-Star	22.42	5.9	166	Yes
Improved A-Star	21.56	5.5	59	No

II. IMPROVEMENT OF LOCAL PATH PLANNING ALGORITHM FOR ARTIFICIAL POTENTIAL FIELD

A. Traditional artificial potential field algorithm

Artificial potential field algorithm is a popular choice among local path planning algorithms. Fig. 4 illustrates the force analysis conducted on the robot within this artificial potential field.

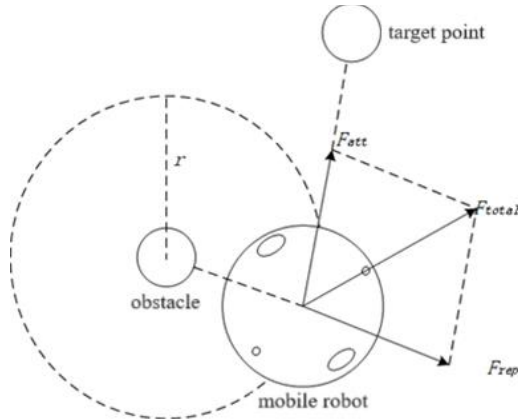


Figure 4. Force analysis diagram of mobile robot

Artificial potential field algorithm's core concept is implemented through the simulation of an imaginary force field, and its theoretical idea can be summarized as follows: the robot is abstracted into a particle with point charge in a virtual force field. The target node generates an attractive potential field that pulls the mobile robot towards it, while obstacles create a repulsive potential field that pushes it away. As the mobile robot draws closer to the target node, the gravitational field intensifies. Similarly, the repulsive force field will also increase when approaching an obstacle. Under the influence of both gravitational and repulsive potential fields,

the mobile robot is propelled towards the target node and finally generates an optimal path that can avoid obstacles autonomously [22].

As the mobile robot enters the obstacle's range of influence, it is simultaneously influenced by both the repulsive force F_{rep} of the obstacle as well as the attractive force F_{att} of the target point, resulting in the total force F_{total} acting on the mobile robot, which determines its actual direction of movement [23]. For the artificial potential field represented in Fig. 4, the virtual force field size can be expressed in terms of the negative gradient of the potential field. Specifically, assuming that mobile robot is located in space m , the repulsive force received by mobile robot continues to increase when it approaches the obstacle, and the gravitational force it receives gradually decreases when it approaches the target point. Thus, the potential field function of mobile robot can be expressed as:

$$\vec{E}_{total}(m) = \vec{E}_{att}(m) + \vec{E}_{rep}(m) \quad (9)$$

In the above formula, $\vec{E}_{total}(m)$ is the total potential field force function of the robot located at m , $\vec{E}_{att}(m)$ is the gravitational potential field function, and $\vec{E}_{rep}(m)$ is the repulsive potential field function. Similarly, below is the definition of the repulsive force field function utilized by mobile robots:

$$\vec{F}_{rep}(m) = -\nabla \vec{E}_{rep}(m) = \begin{cases} \frac{p}{2} k_{rep} \left(\frac{1}{m-m_{pobs}} - \frac{1}{r} \right)^{p-1} \cdot \frac{1}{m-m_{pobs}}, & m-m_{pobs} \leq r \\ 0 & m-m_{pobs} > r \end{cases} \quad (10)$$

In the above equation, k_{rep} is the gain coefficient of the repulsive field, $m-m_{pobs}$ is the Euclidean distance between the current robot position and the obstacle, r is the repulsive radius, and p is an adjustable parameter.

Due to the presence of complex obstacle environments in practical environments, the total force field function can be modified to the sum of the gravitational function and the combined repulsive function, namely:

$$\vec{E}_{total}(m) = \vec{E}_{att}(m) + \sum_{i=1}^n \vec{E}_{rep}(m) \quad (11)$$

The net force experienced by the mobile robot at point m in space can be expressed as:

$$\vec{F}_{total(m)} = -\nabla \vec{E}_{total}(m) = \vec{F}_{att}(m) + \sum_{i=1}^n \vec{F}_{rep}(m) \quad (12)$$

B. Improvement of artificial potential field algorithm

Through the above analysis, it can be seen that the artificial potential field algorithm has the advantages of easy implementation and high performance, but it is also prone to the problem of

$$\vec{E}_{rep}(m) = \begin{cases} \frac{1}{2} k_{rep} \left(\frac{1}{m-m_{pobs}} - \frac{1}{r} \right)^2 (m-m_{end})^p, & m-m_{pobs} \leq r \\ 0 & m-m_{pobs} > r \end{cases} \quad (13)$$

In the above formula, k_{rep} is the repulsion field gain coefficient, $m-m_{pobs}$ is the Euclidean distance between robot position and the obstacle, r is the repulsion radius, and p is an adjustable parameter. Based on the traditional gravitational potential field function, the relative position

unreachable target points, and it cannot play a good role in identifying and avoiding local dynamic obstacles [24]. To address these limitations of the traditional artificial potential field algorithm, this paper proposed solutions. Firstly, the repulsion field parameters were modified to resolve the problem of unreachable target points. Secondly, to enable the algorithm to handle dynamic obstacles, a dynamic potential field function was constructed. This approach solved the problem of dynamic obstacle avoidance.

1) Correction of repulsion field parameters

Although the traditional artificial potential field algorithm is relatively easy to implement, when there are obstacles around target point and target point is within the range of obstacles influence, there may be a phenomenon where the target point is unreachable. To make the magnitude of the repulsive force change as the gravitational force changes with the distance, the repulsive force function was modified by referring to the gravitational potential field function. By introducing the relative position $(m-m_{end})^p$, the repulsive force decreases continuously when it approaches the target point. The modified repulsion field function can be expressed as:

$(m-m_{end})^p$ was introduced and the repulsive field parameters are adjusted. This made the repulsive force of the mobile robot decreased as it approached the target point.

With the negative gradient of the repulsive force field function signifying its intensity, the repulsive force can be expressed as:

$$\vec{F}_{rep}(m) = -\nabla \vec{E}_{rep}(m) = \begin{cases} \vec{F}_{rep1} + \vec{F}_{rep2} & , m - m_{pobs} \leq r \\ 0 & , m - m_{pobs} > r \end{cases} \quad (14)$$

Where:

$$\vec{F}_{rep1} = k_{rep} \left(\frac{1}{m - m_{pobs}} - \frac{1}{r} \right) \frac{(m - m_{end})^p}{m - m_{pobs}^2} \quad (15)$$

$$\vec{F}_{rep2} = -\frac{p}{2} k_{rep} \left(\frac{1}{m - m_{pobs}} - \frac{1}{r} \right)^2 (m - m_{end})^{p-1} \quad (16)$$

The repulsive force \vec{F}_{rep1} points to the direction of the robot from the obstacle. The repulsive force \vec{F}_{rep2} points to the target point from the robot.

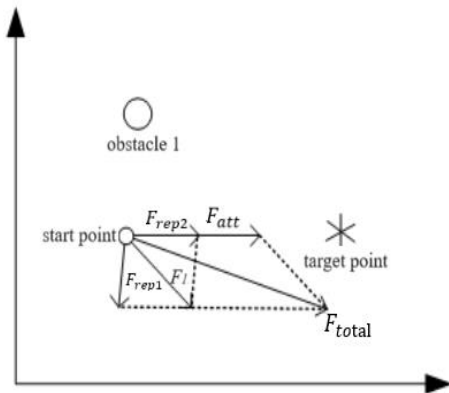


Figure 5. Modified repulsion field parameters force analysis

The force analysis after adjusting the repulsion field parameters is shown in Fig. 5, where the x-axis and y-axis represent the distance traveled, measured in meters.

2) Construction of dynamic force field

The artificial potential field being a blend of gravitational and repulsive fields, therefore, it is logical to divide the dynamic potential field into two sections: a gravity field based on relative velocity and a repulsion field based on relative velocity.

Gravity field based on relative velocity: in an indoor unstructured environment, a mobile robot faces the challenge of path planning in the presence of dynamic obstacles. By adding a relative velocity term to the traditional gravitational potential field function, a dynamic gravitational potential field function is formed. The function for the relative velocity gravitational field can be formulated as:

$$\vec{E}_{att}(m, v) = \frac{1}{2} k_{att} (m - m_{end})^p + \frac{1}{2} k_{att} (v - v_{end})^p \quad (17)$$

In the above formula, $(v - v_{end})$ is the relative speed of the mobile robot to the target point in space m . k_{att} is the gravitational gain coefficient, p is the adjustable parameter, m_{end} is the endpoint coordinates (x_{end}, y_{end}) , m is the robot current point coordinates (x, y) , and $(m - m_{end})$ represents the Euclidean distance between point m and the end point.

Then the gravity function is expressed as:

$$\vec{F}_{att}(m, v) = -\nabla \vec{E}_{att}(m) = \frac{P}{2} k_{att} (m - m_{end})^{p-1} + \frac{P}{2} k_{att} (v - v_{end})^{p-1} \quad (18)$$

The gravity $\vec{F}_{att}(m)$ points to the target point, and the size of the velocity gravity function $\vec{F}_{att}(v)$ is related to the relative velocity between mobile robot and target point.

Repulsion field based on relative velocity: similar to the dynamic gravitational force field, the relative velocity term is also added in the

construction of the dynamic repulsive field. Additionally, considering that there may be dynamic obstacles in the environment, the relative velocity based on obstacles is added. Thus, the repulsion field function based on relative velocity is as follows:

$$\vec{E}_{rep}(m, v) = \begin{cases} \vec{E}_{rep}(m) + \vec{E}_{rep}(v), & m - m_{pobs} \leq r \text{ and } 0 \leq v \\ \vec{E}_{rep}(m) & , m - m_{pobs} \leq r \text{ and } 0 \leq v \\ 0 & , m - m_{pobs} > r \end{cases} \quad (19)$$

In which,

$$\vec{E}_{rep}(m) = \frac{1}{2} k_{rep} \left(\frac{1}{m - m_{pobs}} - \frac{1}{r} \right)^2 (m - m_{end})^p \quad (20)$$

$$\vec{E}_{rep}(v) = k_{att} (v - v_{pobs})^e \quad (21)$$

$\vec{E}_{rep}(m)$ is the repulsion field function of the mobile robot in space m , $\vec{E}_{rep}(v)$ is the velocity field function. $(v - v_{pobs})$ represents the moving speed of the mobile robot relative to the obstacle. e represents a unit vector. Then the repulsion function is:

$$\vec{F}_{rep}(m, v) = -\nabla \vec{E}_{rep}(m, v) = \begin{cases} \vec{F}_{rep}(m) + \vec{F}_{rep}(v), & m - m_{pobs} \leq r \text{ and } 0 \leq v \\ \vec{F}_{rep}(m) & , m - m_{pobs} \leq r \text{ and } v \leq 0 \\ 0 & , m - m_{pobs} > r \end{cases} \quad (22)$$

In which, $\vec{F}_{rep}(m) = \vec{F}_{rep1} + \vec{F}_{rep2}$:

$$\vec{F}_{rep}(v) = -k_{rep} e \quad (25)$$

$$\vec{F}_{rep1} = k_{rep} \left(\frac{1}{m - m_{pobs}} - \frac{1}{r} \right) \frac{(m - m_{end})^p}{m - m_{pobs}} \quad (23)$$

$$\vec{F}_{rep2} = -\frac{p}{2} k_{rep} \left(\frac{1}{m - m_{pobs}} - \frac{1}{r} \right)^2 (m - m_{end})^{p-1} \quad (24)$$

For the purpose of confirming the validity of the improved algorithm, a 30m×30m grid was constructed in the MATLAB environment, and two sets of experimental comparisons were carried out to analyze the improved artificial potential field algorithm, comparing it with the traditional version. The first set of experiments selected the grid map environment in Fig. 1 for simulation comparison. The unit of horizontal and vertical

axes is m. As depicted in Fig. 6, these are the experimental results.

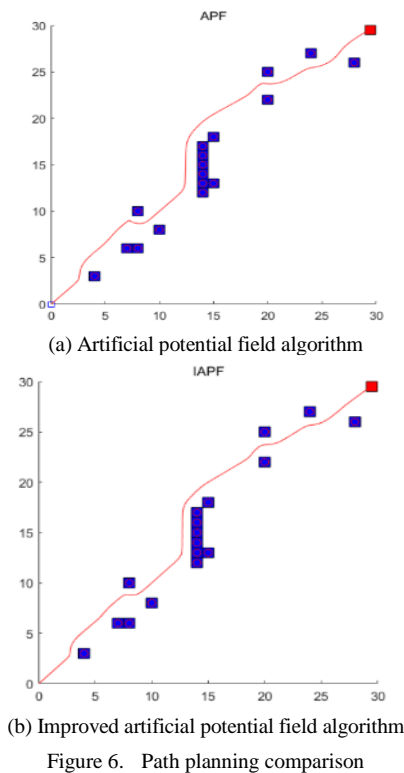


Figure 6. Path planning comparison

The second set of experiments was simulated, using red circles to represent obstacles set up, to test the path planning effectiveness of the two algorithms when encountering local obstacles.

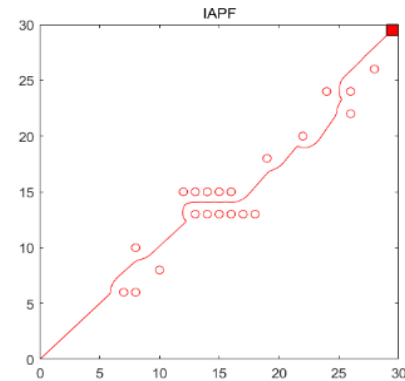
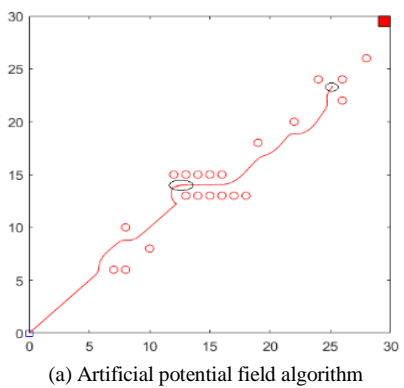


Figure 7. Complex obstacle test comparison

Fig. 6 reveals that in a static setting, the improved artificial potential field algorithm achieves smoother path planning and more precise obstacle detection, outperforming the traditional approach. However, in the dynamic environment portrayed in Fig. 7, the traditional algorithm fails to navigate to the target due to challenges in obstacle recognition. The lengthy path and extended runtime depicted in Fig. 7(a) are symptomatic of the complex obstacle environment, which poses a challenge for the traditional algorithm. Fortunately, the enhanced algorithm overcomes this limitation.

As Table 2 indicates, by modifying the repulsion field parameters, the challenge of inaccessible target points was conquered, the oscillation phenomenon was effectively eliminated, compared with the traditional artificial potential field algorithm. Its running time was reduced by 13.92%, the path length was reduced by 4%. By way of comparative experiments, the efficacy of the improved artificial potential field algorithm was thoroughly validated.

TABLE II. COMPARISON RESULTS OF IMPROVED ALGORITHM

Experiment Name	Algorithm	Path length/m	Run time/s	Number of cycles
Path planning testing	APF	49.970710	6.186677	447
	IAPF	48.003037	5.430491	440
Complex obstacle testing	APF	∞	∞	∞
	IAPF	51.519690	6.801836	451

III. HYBRID ALGORITHM SIMULATION EXPERIMENT AND RESULT ANALYSIS

A. Principle of hybrid algorithm

In indoor unstructured complex environments, neither the artificial potential field algorithm nor A-star algorithm is capable of accomplishing optimal path planning on its own. Consequently, this paper integrated these two path planning algorithms into a hybrid solution that combines the advantages of both and can complete the optimal path planning task.

During the implementation process of the hybrid path planning algorithm, the following two problems should be considered: Firstly, when the mobile robot does not enter the obstacle's radius of influence, the optimized A-star algorithm is utilized to obtain global initial paths for global path planning; Secondly, utilizing this comprehensive global path as a foundation, it is necessary to determine whether there are any reserved nodes generated by A-star algorithm within the obstacle's range of influence. If there are, further reductions should be made. Fig. 7 depicts the model for the hybrid path planning algorithm:

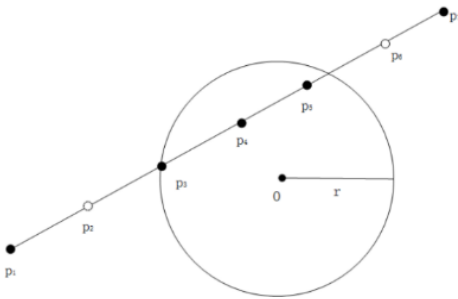


Figure 8. Hybrid algorithm model diagram

In Fig. 8, (p_1, \dots, p_i) are the path intermediate node of the A-Star algorithm, and r is the radius of influence of the obstacles. Among them, $p_1, p_2, p_3, p_4, p_5, p_6, p_7$ are the reserved nodes of the optimized A-star algorithm.

Assuming that the robot at time t is located at point p_1 , upon advancing to point p_3 , the mobile robot comes under the influence of the artificial potential field algorithm. Since points p_4 and p_5

fall within this influence, they are disregarded, and the next node p_7 is taken as the target point.

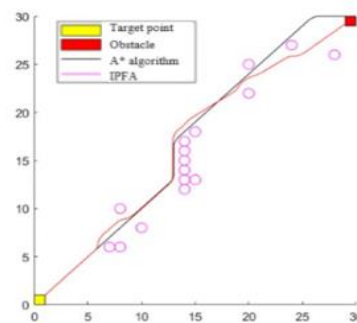
The hybrid path planning algorithm proceeds in the following execution stages:

- 1) Initialize map parameters;
- 2) Carry out global path planning utilizing the A-Star algorithm, while documenting and storing the path nodes for future reference;
- 3) Use node pruning strategy to retain key path nodes;
- 4) Treat the key path nodes as local target points in turn. If the key target node is within the radius of the obstacle, the node is deleted and the next key node is selected as the target node;
- 5) With the utilization of the improved artificial potential field algorithm, the robot systematically traverses from its current location to the next sub-target, ensuring accurate path planning;
- 6) Check if the robot has completed its journey to the final target node. Stop if it has; otherwise, repeat step 5 for further route calculation.

B. Simulation of experimental results of hybrid algorithm

1) Experimental results in static environment

The experiment used MATLAB to conduct simulation tests on the hybrid path algorithm. The experimental environment was also set as the grid map model depicted in Fig. 1. The experiment was carried out in both dynamic and static environments, grouped according to whether the obstacles are movable or not. The figure below demonstrates the experimental results.



(a) the improved A-Star and the improved artificial potential field

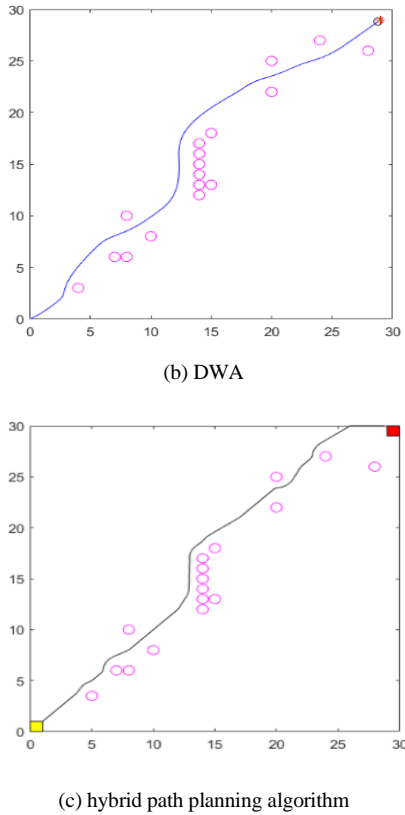


Figure 9. Static path comparison diagram

The above three sets of experiments were conducted in a static environment to compare the path planning information generated by the improved A-star algorithm, the improved artificial potential field algorithm, DWA algorithm, and the hybrid algorithm. The comparison was based on their respective planning path lengths, search path durations and ability to handle dynamic obstacles.

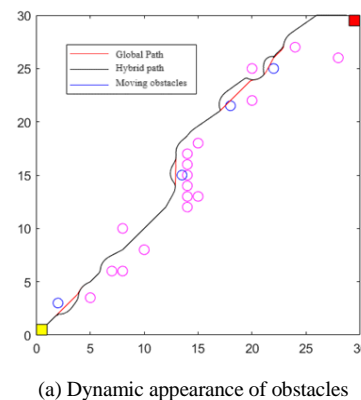
As evident from Table 3 and Fig. 9, in the context of identical obstacles, the A-Star algorithm demonstrates an ability to plan a short path with rapid search speed during the path planning process, but it does not have the ability to dynamically avoid obstacles. Despite its longer planned path and increased search duration, the artificial potential field algorithm boasts the crucial capability of dynamically steering clear of obstacles, making it a practical choice for complex indoor navigation scenarios. By fusing the benefits of the two algorithms, the hybrid approach achieves not only a shorter search path and time but also the flexibility to handle dynamic obstacles effectively.

TABLE III. ALGORITHM COMPARISON IN STATIC ENVIRONMENT

Algorithm	Path length/m	Search time/s	Does the algorithm have the ability to handle dynamic obstacles
A-Star	45.36	6.72	No
IAPF	48.00	10.43	Yes
DWA	48.86	28.21	Yes
Hybrid algorithm	46.54	8.14	Yes

2) Experimental results in dynamic environment

The path planning experiment of the hybrid algorithm was conducted in a 30m×30m environment. In the dynamic environment, the parameters for obstacle avoidance were set to include a step increment of 0.1, a gravitational and velocity gain of 3, an obstacle detection radius of 3 units, and a repulsive gain of 5. The predefined obstacle was programmed to traverse a path from the point (12, 17) to (16, 17). The figure below demonstrates the experimental results.



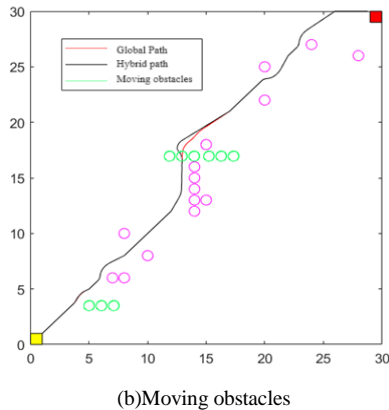


Figure 10. Dynamic path planning diagram

The purple circles in Fig. 10(a) represent static obstacles that already exist, while the blue circles represent dynamic obstacles that appear randomly. In Fig. 10(b), green circles represent persistent dynamic obstacles, which move left and right between positions with ordinates of 3 and 17. These images compared the path under the hybrid algorithm with the static simulated global path to show the impact of the introduction of dynamic and moving obstacles on the return of the global path. In Fig. 10(a), the hybrid algorithm can effectively avoid dynamically appearing obstacles in the simulated indoor environment and return to the global path, ensuring the real-time nature of the path planning task. Mobile obstacles were introduced in Fig. 10(b). Mobile robot effectively avoided dynamic obstacles and returned to the global path, which effectively verified the effectiveness of the improved hybrid algorithm. Additionally, this enhancement significantly improved the real-time performance of path planning.

C. Verification of hybrid algorithm experiment in real environment

The robot platform in this paper was built on the Hands-free mobile robot platform. RPLIDAR A1 lidar was selected as the main ranging sensor. To steer the mobile robot's motions precisely, the OpenRE Board controller was selected as the primary control mechanism. According to the composition structure of the Handsfree_Stone_V3 mobile robot, the various hardware parts were assembled. The finished assembly of Handsfree_Stone_V3 is shown in Fig. 11.

The physical environment verification was conducted in a room with dimensions of 4.5 meters in length and width. The laboratory was equipped with obstacles, and the test commenced from the doorway position. As shown in Fig. 12.

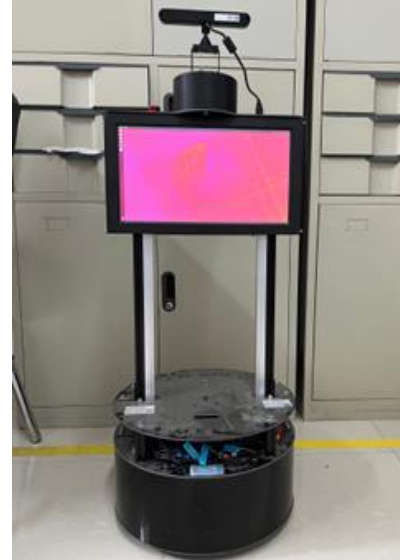
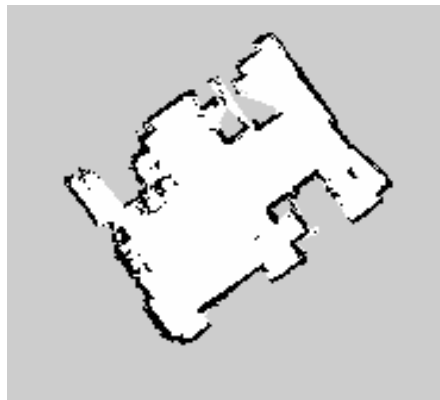


Figure 11. Hands-free robot platform



Figure 12. Actual test scenario

This paper used Gmapping to complete the mapping of the actual environment of the Hands-free robot. The mapping results and mapping parameters are shown in Fig. 13:



(a)Actual environmental mapping

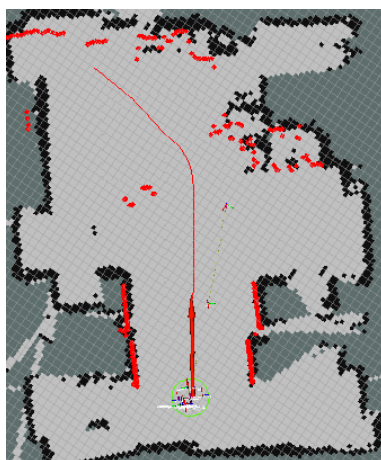
```

315_map.yaml (~/handsfree/handsfree_ros)
打开(O) [icon]
image: 315_map.pgm
resolution: 0.050000
origin: [-10.000000, -10.000000, 0.000000]
negate: 0
occupied_thresh: 0.65
free_thresh: 0.196
    
```

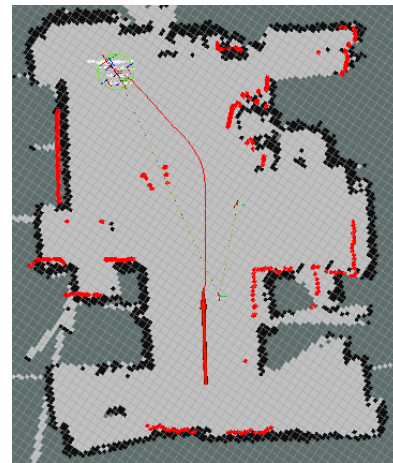
(b)Actual environmental mapping parameters

Figure 13. Actual scene construction effect

After completing the mapping of the actual environment as mentioned above, the next step is a comparative analysis of the path planning prowess of the traditional A-Star hybrid DWA algorithm and the improved A-Star hybrid improved artificial potential field algorithm presented herein. The comparison was executed in a real-life setting, mirroring actual environmental conditions. The figure below demonstrates the experimental results.

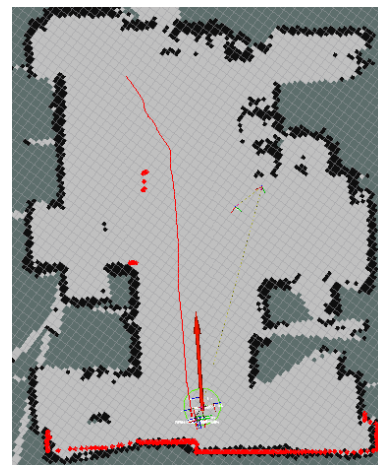


(a)Starting position



(b)Ending position

Figure 14. A-Star Hybrid DWA algorithm path planning



(a)Starting position



(b)Ending position

Figure 15. Improved A-Star hybrid improved artificial potential field algorithm

The navigation effects in Fig. 14 and Fig. 15 and the data in Table 4 show that, under the

condition of setting the same starting and ending points, by comparing the path length, search time and passing nodes number of the two path planning algorithms, it can be found that the hybrid algorithm proposed in this paper reduced path planning length by 10.3%, reduced the

running time by 12.5%, and passed through 34 less redundant nodes. This proved that in real environments, the hybrid algorithm introduced in this paper offers distinct advantages in path planning over the traditional hybrid algorithm.

TABLE IV. Results of algorithm comparison in real environment

Path planning algorithm	Path length/m	Number of nodes passed through	Search time/s
A-Star Hybrid DWA	3.66	126	54.42
Hybrid algorithm in this paper	3.24	92	48.36

IV. CONCLUSIONS

The objective of this paper is to primarily identify and enhance the weaknesses in the conventional A-Star algorithm and the artificial potential field algorithm, thereby optimizing their performance. Firstly, the heuristic factor of A-star algorithm was adjusted, and its redundant nodes were eliminated using the node deletion strategy. Simultaneously, the path turning points of A-star algorithm were smoothed. The search time was shortened effectively. Secondly, the deficiencies of the artificial potential field algorithm were addressed in static and dynamic environments separately. In the static environment, the target unreachable problem is solved by modifying the repulsion field parameters. In the dynamic environment, the relative speed term was introduced so that the speed of the mobile robot becomes smaller when approaching the obstacle and becomes larger when it is further away. The simulation results indicated that the hybrid algorithm efficiently addressed the path planning dilemma for mobile robots within a complex and unstructured indoor space. The improved algorithm's running time was reduced by 13.92%, and the planned path length was reduced by 4%. In the part of actual environment verification, the path planning results between the traditional hybrid algorithm and the improved algorithm was compared. The results showed that the path planning length was reduced by 10.3%, the running time was decreased by 12.5%, and 34 redundant nodes were eliminated by the hybrid algorithm presented in this paper, demonstrating

greater efficiency than the traditional hybrid algorithm.

ACKNOWLEDGMENT

The authors wish to thank the cooperators. This research is partially funded by the Project funds in Shaanxi province University Student Innovation and Entrepreneurship Fund Project (S202310702059).

REFERENCES

- [1] HUO Jiajia, LIU Yu, ZHANG Xuanyi, et al. Research on Obstacle Avoidance and Path Optimization of Intelligent Vehicle [J]. Shandong Industrial Technology, 2017(11):163.
- [2] XIN Peng. Research on Mobile Robot Path Planning Based on A* Algorithm [D]. Hebei University of Technology, 2022.
- [3] REN Hongge, HU Hongchang, Shi Tao. Dynamic Path planning of Mobile Robot based on improved ant Colony Algorithm [J]. Modern Electronics Technique, 2021, 44(20):182-186. (in Chinese)
- [4] KANG Chengbo. Research on Autonomous localization and Navigation System of logistics robot based on Laser SLAM [D]. Shanghai University of Engineering Science, 2020.
- [5] Fox D, Burgard W, Thrun S. The dynamic window approach to collision avoidance[J]. IEEE Robotics & Automation Magazine, 2002, 4(1): 23-33.
- [6] ZHU Manman, DU Yu, ZHANG Yonghua, et al. Local Path planning for Intelligent Vehicle based on Fuzzy Logic [J]. Journal of Beijing Union University, 2016, 30(04):29-32.
- [7] Peter E H, Nils J N, Betram R. A Formal Basis for the Heuristic Determination of Minimum Cost Paths[J]. IEEE Transactions on Systems Science and Cybernetics, 1968, 4(2): 100-107.
- [8] HUO Fengcai, CHI Jin, HUANG Zijian, et al. Mobile Robot path planning Algorithm Review (Information Science Edition) [J]. Journal of Jilin University, 2019, (10):19-21.
- [9] GAO Mindong, ZHANG Yani, ZHU Lingyun. Bidirectional aging A* Algorithm for Robot Path

- Planning [J]. Application Research of Computers, 2019, 36(3):792-795.
- [10] GU Chen. Application of Improved A* Algorithm in Robot Path Planning [J]. Electronic Design Engineering, 2014, 22(19):96-98.
- [11] WANG Shuaijun, HU Likun, WANG Yifei. Path planning of Indoor Mobile Robot based on improved D~* Algorithm [J]. Computer Engineering and Design, 2019, 41(4):1118-1124. (in Chinese)
- [12] Duchon F, Babinec A, Kajan M, et al. Path Planning with Modified a Star Algorithm for a Mobile Robot[J]. Procardia Engineering, 2014, 96(96):59-69.
- [13] Liu J, Yang J, Liu H, et al. An Improved Ant Colony Algorithm for Robot Path Planning[J]. Soft Computing, 2017, 21(19):5829-5839.
- [14] Kaplan A, Kingry N, Uhing P, et al. Time-Optimal Path Planning with Power Schedules for a Solar-Powered Ground Robot [J]. IEEE Transactions on Automation Science and Engineering, 2017, 14(2):1235-1244.
- [15] Xu X L, Pan W, Huang Y B. Dynamic Collision Avoidance Algorithm for Unmanned Surface Vehicles via Layered Artificial Potential Field with Collision Cone[J]. Journal of Navigation, 2020, 73(6):1306-1325.
- [16] Zhang C. Path Planning for Robot based on Chaotic Artificial Potential Field Method[C]. //International Conference on Advanced Engineering and Technology, 2018, 317.
- [17] XU Fei. Research on Obstacle Avoidance and Path Planning of Robots Based on Improved Artificial Potential Field Method [J]. Computer Science, 2016,43(12):293-296.
- [18] ZHANG Qiang, LU Shouyin, ZHANG Jiarui, et al. Path planning of inspection robot based on Safety A* algorithm and improved artificial potential field method [J]. Computer Age, 2022, (11):29-33+37.
- [19] ZHANG Shengnan. Research on Path Planning and Tracking Algorithm of Mobile Robot [D]. Heilongjiang University, 2021.
- [20] ZHOU Shibo. Path planning of wheeled robot based on improved A* algorithm and artificial potential field method [D]. Taiyuan University of Technology, 2021.
- [21] LV Jindou. Research on Robot Dynamic Path Planning Based on Improved A~* Potential Field Method [D]. Xi'an University of Architecture and Technology, 2020.
- [22] ZHI Jin Zhu. Research on Path Planning of Indoor Mobile Robot in Dynamic Environment [D]. Xi'an Technological University, 2021.
- [23] LU Jian. Path Planning and Navigation of Indoor Mobile Robot [D]. Fujian University of Technology, 2022.
- [24] Qi B, Li M, Yang Y, et al. Research on UAV path planning obstacle avoidance algorithm based on improved artificial potential field method[J]. Journal of Physics: Conference Series, 2021, 1948(1): 14-16